# Evaluating Heat Vulnerability in Kinshasa, DR Congo: A GIS-Based Study Using Open-Source Geospatial Data

**Christian C. Oluoma[1*] Michael B. Onyango[2,3], Godfrey Nengai[4] Oluwafemi B. Obe[5] and Jumoke Omodeni[6]**

*[1]Department of Geoinformatics & Surveying, University of Nigeria, Nigeria*

*[2]Department of Land Resources Management and Agricultural Technology, University of Nairobi, Kenya*

*[3] Center for Ecosystem Restoration, Kenya*

*[4]Department of Physics, University of Dar es Salaam, Tanzania*

*[5]School of Geography, University College, Ireland*

*[6]Center of Learning, and Research, Eco Science Generation Initiative, Nigeria*

**Corresponding author: benjamin.obe@ucdconnect.ie*

https://doi.org/10.62049/jkncu.v5i2.304

## Abstract

*Heat stress poses significant and unexpected dangers, particularly in regions like Sub-Saharan Africa, where comprehensive heat risk assessments are lacking. In Central Africa, there has been little effort to investigate intra-city heat risk patterns due to limited data and computational resources at the institutional level. This study addresses this gap by synthesizing open-source geospatial datasets, including high-resolution land surface temperature data from Landsat, to map health-related heat risk in Kinshasa, DRC. Using a quantitative risk framework that integrates hazard, exposure, and vulnerability components, the analysis was conducted in open-source QGIS software and Google Earth Engine. The findings reveal a heat risk gradient that systematically decreases outward from the city center. Urban areas exhibit medium to high heat risk, while suburban and rural areas display low and very low risk. This pattern underscores the influence of factors such as the distribution of socioeconomic status, age demographics, population density, and vegetation coverage on heat risk. The study offers valuable insights for policymakers to develop targeted heat adaptation and mitigation strategies tailored to the most vulnerable areas of Kinshasa.*

**Keywords:** Heat Risk; Land Surface Temperature; Vulnerability Assessment; Climate Change; GIS

## Introduction

The climate crisis is the defining environmental challenge of the 21st century. For the first time in human history, climate changes are occurring at a pace that exceeds natural historical variations (World Bank, 2018). Between 2011 and 2020, the Earth's surface temperature was approximately 1.1 °C higher than the late 19th-century average, making it the warmest period in the past 100,000 years (IPCC, 2021). This increase in global temperature, largely driven by anthropogenic greenhouse gas emissions, is fuelling global warming.

Global warming is expected to intensify the frequency and severity of extreme heat events, including heatwaves and droughts (Perkins et al., 2012). These events pose significant threats to human health (Campbell et al., 2018), biodiversity (Harris et al., 2018), and global food security (Deryng et al., 2014), while also leading to substantial economic losses (Forzieri et al., 2018) and ecosystem disruptions. Heatwaves are particularly dangerous due to their variability in duration and intensity. Prolonged exposure to extreme heat can result in heat stress, which may cause dehydration (Costello et al., 2018), heat cramps (Hajat et al., 2010), and, in severe cases, fatalities from respiratory or cardiovascular failure (Oudin et al., 2011). These heat related issues pose greater risk in regions with high vulnerability and exposure to heats, especially regions in lower latitudes.

Sub-Saharan Africa is one of the regions that is most vulnerable to the effects of heat waves, due to its hot a combination of hot and humid climate conditions, rapid urbanization, and limited capacity for adaptation at both the institutional and community levels (Ayal 2021; Epule et al. 2021). Many cities in the region are already struggling to cope with rising heat stress, underscoring the urgent need for climate adaptation and mitigation strategies that are responsive to local contexts. Major urban centres such as Abidjan, Abuja, Accra, Addis Ababa, Cape Town, Dar es Salaam, Durban, Harare, Johannesburg, Juba, Kampala, Kinshasa, Lagos, Luanda, Lusaka, Mogadishu, Nairobi, Pretoria, Windhoek, Dodoma, Maputo, and Jinja are experiencing growing challenges related to extreme heat. One key factor is the urban heat island (UHI) effect, which occurs when urban areas become significantly warmer than surrounding rural areas due to dense infrastructure, limited vegetation, and altered surface energy balances. High levels of urbanization intensify this effect, thereby increasing the risks associated with heatwaves (Odame et al., 2018; Patz et al., 2005; Tan et al., 2010).

Recent studies across Africa have shown that extreme heat stress is not uniformly distributed within urban areas. For example, Obe et al., (2023) found that in Lagos, Nigeria, heat risk is predominantly concentrated in densely populated, low-income neighborhoods. Similarly, Van De Walle et al., (2022) highlighted that the absence of vegetation exacerbates heat exposure in compact urban settlements in tropical African cities. Moreover, studies from other global contexts also reveal that heat extremes often disproportionately affect lower-income or socially disadvantaged communities. For instance, Zheng et al. (2020) found that the northern Jiangxi province of China, a heavily populated suburban region, faced the highest heat risk. Similarly, Maragno et al. (2020) reported that different urban forms in Padova, Italy, were associated with varying degrees of vulnerability. In Brazil, Lapola et al. (2019) demonstrated a strong link between socioeconomic inequality and heat exposure, with the poorest neighborhoods bearing the greatest risk. These patterns reflect the fact that heat hazard risk is largely shaped by the interaction of hazard intensity, exposure, and vulnerability—all of which can vary considerably even within the same city (Obe et al., 2023a; Hu et al., 2019). Vulnerability indicators such as age demographics, socioeconomic status, housing

quality, and health conditions often differ across neighborhoods (Kang et al., 2020). For example, in Lahore, Pakistan, Rana et al. (2022) found that households in informal settlements had limited adaptive capacity, making them especially susceptible to extreme heat. Given this uneven distribution of risk factors, detailed assessments of exposure and vulnerability are critical for developing effective and equitable heat risk management strategies (Abrar et al., 2022).

The growing frequency and intensity of heatwaves projected by climate models (Luber & McGeehin, 2008) make these findings even more concerning. While the World Meteorological Organization (WMO, 2023) notes that African countries have the capacity to anticipate heatwaves, the lack of high-resolution, field-based meteorological data limits the ability to monitor, document, and respond to their impacts. This is particularly worrying in Central Africa, where research on heat waves and associated risks is significantly lacking, particularly in rapidly growing urban areas.

In recent years, efforts have been made to address this knowledge gap in parts of Sub-Saharan Africa. For instance, Morakinyo et al. (2024) used ERA5-HEAT reanalysis data to examine long-term trends in heat stress across Nigeria, identifying predominantly positive trends over a 40-year period. However, the relatively coarse spatial resolution of ERA5-HEAT data restricts its ability to capture heat stress variations within urban areas. Similarly, while satellite-based land surface temperature (LST) data—such as Moderate Resolution Imaging Spectroradiometer (MODIS)—is widely used in heat-health assessments, its resolution remains insufficient for detailed intra-urban analysis (He et al., 2019). To address these limitations, some studies have begun integrating advanced modelling with geospatial datasets. For example, Obe et al. (2023) applied the Weather Research and Forecasting (WRF) model in Lagos to simulate Humidex-based heat stress during a specific heatwave. Their approach successfully identified high-risk zones within specific Local Climate Zones. Although this method provides valuable insights, its high computational demands may be impractical for many Central African cities that lack sufficient institutional and technical resources.

Despite these contributions to understanding heat risk patterns across Sub-Saharan Africa, little to no effort has been made to investigate heat risk patterns in the Central African region. This study, therefore, represents a preliminary attempt to assess heat risk in Kinshasa, DR Congo. The key objective of the study is to conduct a spatial assessment of extreme heat exposure and associated risks in Kinshasa, Democratic Republic of Congo. The specific objectives are: (1) to map the spatial distribution of extreme heat using remote sensing data; (2) to assess the relationship between environmental and socio-demographic variables contributing to heat vulnerability; and (3) to demonstrate a scalable, data-accessible methodology for heat risk assessment in resource-constrained urban settings across Africa. These assessments are necessary for creating responsive, inclusive and practical heat mitigation strategies which will help protect the at-risk populations from the growing heat risks.

## Materials and Methods

### Study Area

Kinshasa (Figure 1) is the capital and largest city of the Democratic Republic of Congo, and one of the fastest-growing megacities in Sub-Saharan Africa. It spans approximately 9,965 km² along the southern banks of the Pool Malebo, with flat, low-lying terrain averaging 300 meters above sea level (Kinyamba et al., 2015). With a population density of 1,462 people per km², Kinshasa is the most densely populated area in the DRC and faces significant heat-related challenges linked to rapid urban growth.

The city has a tropical wet and dry climate, with an annual mean temperature of 26°C. Data from WorldData (2023) indicate that the hottest period runs from February to mid-May, with daily highs exceeding 31°C. USAID (2023) reports a warming trend of 0.17°C per decade over the past 30 years, with the hottest days increasing by about 0.25°C per decade. While seasonal variation is moderate, March to May records the highest average daytime temperatures, contributing to increased heat stress.

Kinshasa's dense urban form and limited vegetation contribute to urban heat island effects, especially in informal settlements. Although the city generates 85% of the country's Gross Domestic Product (GDP), only 13% of the national population resides there (Chirisa et al., 2017). The economy is largely informal, with 97% of workers outside formal employment (AFRISTAT & National Institute of Statistics, 2012; Flouriot, 2013), limiting access to essential services and adaptive capacity.

These geographic, climatic, and socioeconomic characteristics make Kinshasa highly vulnerable to extreme heat, highlighting the need for spatially detailed risk assessments to inform targeted mitigation strategies.

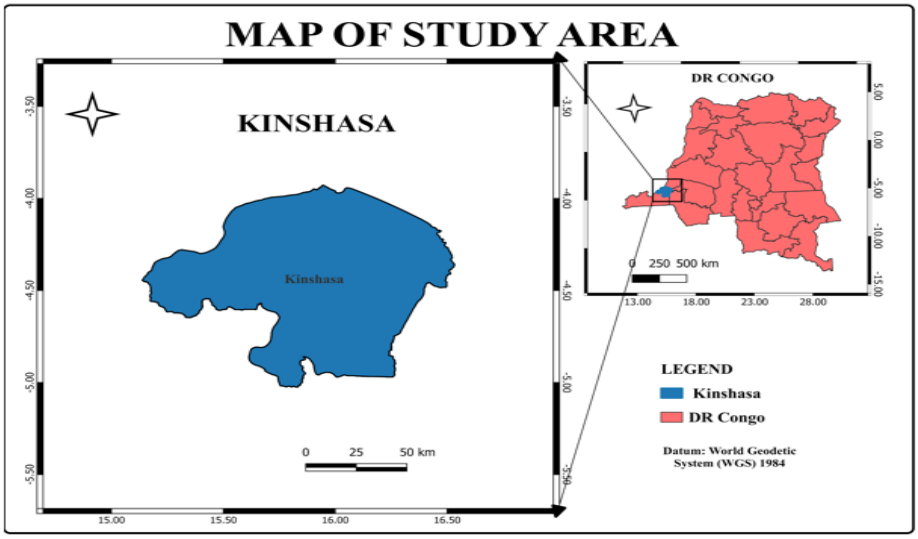


***Figure 1:. Map of Kinshasa, DRC***

**Heat Risk Assessment**

The study employed Crichton's Risk Triangle (Crichton 1999), which is predicated on the spatial coincidence of hazard, exposure, and vulnerability as the foundation for this spatial risk assessment. According to the Intergovernmental Panel on Climate Change (IPCC), climate risk arises from the interaction of three key factors: hazard, exposure, and vulnerability. Hazard refers to the potential occurrence of climate-related physical events or trends that could cause damage and loss, while exposure relates to the presence of assets, services, resources, and infrastructure that could be negatively impacted by these hazards. Vulnerability is the tendency or predisposition of a system or population to be adversely affected by such events (IPCC, 2014). Thus, heat risk can be seen as a function of the heat hazard, exposure and vulnerability components as shown in equation (1) below:

$$Heat\ risk = f(Heat\ hazard, exposure, vulnerability) \qquad (1)$$

In this study, the hazard is the land surface temperature, which is derived from the Landsat imagery. While the spatial pattern of the population density is used as an exposure indicator. Several variables including age, socioeconomic status, distribution of vegetation, and vulnerability were used to represent the vulnerability indicators following Kirsten et al. (2017) and Obe et al. (2023). Table 1 summarizes the data used for this analysis

***Table 1: Summary of Datasets Used for Heat Risk Assessment in Kinshasa***

| Component | Data | Source | Spatial Resolution | Purpose / Description |
|---|---|---|---|---|
| Hazard | Land Surface Temperature (LST) | Landsat-8 (TIRS10), processed via Google Earth Engine | 30 m (resampled to 100 m) | Represents spatial distribution of heat hazard; based on 10-year median composites |
| Exposure | Population Density | WorldPop | ~1 km (30 arc-seconds) | Indicates population distribution to assess exposure to heat |
| Vulnerability | Vulnerable Age Groups | WorldPop | ~100 m (3 arc-seconds) | Identifies children (<10 yrs) and elderly (>65 yrs) as vulnerable population segments |
| | Relative Wealth Index (RWI) | Humanitarian Data Exchange | ~2.4 km (rasterized to 100 m) | Proxy for socioeconomic status; lower values imply higher vulnerability |
| | Vegetation (NDVI) | Landsat-8 (Red & NIR bands), via Google Earth Engine | 30 m (resampled to 100 m) | Proxy for adaptive capacity; higher vegetation reduces heat risk through cooling effects |

**Indicators for the Hazard Component**

Landsat-8 imagery, with a spatial resolution of 30 meters, was utilized as the primary data source for assessing the hazard component. To minimize uncertainty caused by interannual climate variability, we used the median of composite images spanning 10 years (2013-2023), focusing on the months of March, April, and May, with minimal cloud cover. This process was conducted using the Google Earth Engine platform. The Land Surface Temperature (LST) was derived from the Landsat-8 thermal infrared band (TIRS10), using an algorithm for automated LST mapping as developed by Avdan and Jovanovska (2016). The LST was then calculated using the following formula:

$$T_s = \frac{BT}{1 + \left(\frac{\lambda BT}{\rho}\right) ln\, \varepsilon} \qquad (2)$$

where $T_s$is the LST in degrees celsius (∘C), $BT$ is at-sensor Brightness Temperature (∘C), $\lambda$ is the wavelength of emitted radiance, $\varepsilon$ is the emissivity and

$$\rho = \frac{hc}{\sigma} \qquad (3)$$

where $\sigma$ is the Boltzmann constant ($1.38 \times 10^{-23} J/K$), $h$ is Planck's constant ($6.626 \times 10^{-34} Js$), and $c$ is the velocity of light ($2.998 \times 10^{8} m/s$), (Weng et al. 2004).

**Indicators for the Exposure Component**

The grid gross population density data was downloaded from https://www.worldpop.org and used as the exposure component as studies have shown that where there are no people, there is no exposure and consequently, no risk (Buscail et al. 2012; Ma et al. 2023). The population density data acquired at a spatial resolution of 30 arc seconds (~1 km) contains estimated population density at the grid-cell level (Table 1). Its unit, being the number of people per square kilometer, is based on country totals adjusted to match the official United Nations population estimates. Compared to census data, which only offers the total population of each census unit, WorldPop gridded population density data provides higher resolution population distribution information, which is crucial for analyzing heat-related risk (Loughnan et al. 2014; Bao et al. 2015; Ma et al. 2023).

**Indicators for the Vulnerability Component**

*Age Structure Data*

The age structure data, which was acquired from https://www.worldpop.org at a spatial resolution of 3 arc seconds (~ 100 meters) contain estimates of the total number of people per grid square broken down by gender and age groupings. Its units are the estimated number of males/ females in each age group per grid square with country totals adjusted to match the official United Nations population estimates. Studies have shown that certain population groups are more susceptible to heat stress than others. Individuals with chronic illnesses or impairments, the elderly, small children, and those from low-income backgrounds have demonstrated high susceptibility to heat-related illnesses (Hajat & Kosatky 2010; Buscail et al. 2012; Morabito et al. 2015). According to Kenny et al. (2018), due to their bodies' potential incapacity to regulate temperature, older adults and small children are frequently more susceptible to the negative consequences of heat stress. In this study, we consider people within the age group of above 65 years and below 10 years to be the most vulnerable to heat risk, as demonstrated by Obe et al. (2023).

*Relative Wealth Index Data*

The relative wealth Index (RWI) data, which was downloaded from https://data.humdata.org, estimates the relative standard of living across 93 low- and middle-income countries using de-identified connectivity data, satellite imagery, and other nontraditional sources. The dataset is provided as point data, with each point representing an area approximately 2.4 km in size. For this study, the vector data was rasterized to a 100-meter spatial resolution. Socioeconomic status was inferred using RWI values, based on the assumption that the poorest neighborhoods tend to be the most vulnerable to heat risk (Lapola et al. 2019; Adegun et al. 2021). In contrast, wealthier areas are considered less vulnerable due to better access to adaptive infrastructure such as air conditioning and reliable electricity.

*NDVI: Landsat Data*

The Normalized Difference Vegetation Index (NDVI) is a widely recognized remote sensing metric used to assess vegetation health and density. It is calculated from the reflectance values of specific spectral bands in satellite imagery, particularly the red (R) and near-infrared (NIR) bands.

Vegetation and water coverage are often associated with lower temperatures and reduced heat-related mortality, as they can absorb and mitigate heat (Bowler et al. 2010; Zhang et al. 2016; Ma et al. 2023). Therefore, vegetation indices like NDVI can serve as important indicators of vulnerability to heat (Defries et al. 1994; Xu et al. 2006). In this study, the spatial pattern of NDVI was generated using the Google Earth Engine cloud computing platform, applying equation (4) to the reflectance values from the red (R) and near-infrared (NIR) bands of the landsat-8 composite image:

$$NDVI = \frac{(NIR - R)}{(NIR + R)} \quad (4)$$

Vegetation is selected as a key indicator of vulnerability because it provides evaporative cooling, which helps mitigate the acute heat stress commonly observed in urban areas (Van de Walle et al. 2022; Obe et al. 2023). The NDVI represents the percentage of healthy vegetation in the area, which is crucial for understanding the region's resilience to heat stress.

## Method of Analysis

The study was conducted through a series of systematic steps, as illustrated in the framework presented in Figure 2. The analysis began by extracting the LST and NDVI from a ten-year composite Landsat-8 image (2013-2023) using the Google Earth Engine cloud computing platform. LST was utilized to represent the hazard component, while the vulnerability component was assessed through several indicators: the vulnerable age group, the Relative Wealth Index (RWI), and the NDVI. The exposure component was represented by gridded population density data.

To evaluate the overall heat-related risk, we employed Crichton's risk triangle framework, which integrates the three key components—heat hazard, heat exposure, and heat vulnerability. By multiplying these components, we were able to generate a comprehensive map of heat-related health risks, identifying areas where the population is most at risk.

### Normalization

To ensure uniformity and comparability across datasets, each image was resampled to a consistent 100 m resolution. The results were then normalized to a scale between 0.1 and 0.9 using Equation (5) following Dong et al. (2020). This step was crucial for minimizing errors that could arise from combining multiple data sources with varying spatial resolutions, thereby enhancing data compatibility and facilitating subsequent aggregation.

$$X^{!} = 0.1 + \frac{(X - X_{min})}{(X_{max} + X_{min})} * (0.9 - 0.1) \quad (5)$$

where $X^{!}$ the standardized value, $X$ is the original value, and $X_{min}$ and $X_{max}$ represent the minimum and maximum values of the original indicators, respectively.

### Vulnerability Layer

The vulnerability layer was estimated using three key indicators: the vulnerable age group, the NDVI, and the RWI. It is important to note that both NDVI and RWI inversely correlate with vulnerability, as higher vegetation coverage and wealth reduce heat risk (adaptive capacity). Therefore, the values for NDVI and

RWI were inverted following Kerstin et al. (2017). Similar to the approach utilized in previous studies, the vulnerability layer shown in equation (6) was calculated as an equally weighted linear sum of these three sub-indicators (Dong et al. 2014; Obe et al. 2023).

$$V = \frac{(va - NDVI - RWI)}{3} \qquad (6)$$

Where $V$ is the vulnerability layer, $va$ is the population of the vulnerable age group, $RWI$ is the relative wealth index, and $NDVI$ is the vegetation index.

### Aggregate Risk Layer

The final heat risk layer (FHRL) was computed by multiplying the normalized and equally weighted components of hazard, exposure, and vulnerability as shown in equation (7). Previous studies such as Chen et al. (2021), Ma et al. (2023), Obe et al. (2023) have shown the multiplicative principle to capture more nuanced interactions between components than the additive principle.

$$FHRL = Hazard * Exposure * Vulnerability \qquad (7)$$

Where $FHRL$ is the resulting final heat risk layer, which is subsequently classified using Jenks Natural Breaks for better visualization and interpretation of risk distribution.

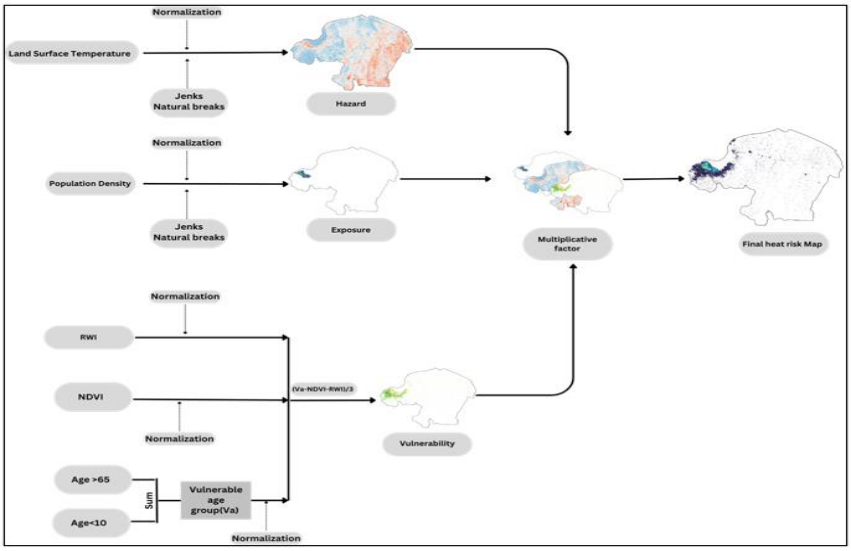


*Figure 2: Methodology framework to assess heat risk in Kinshasa.*

## Results and Discussion

### LST Spatial Pattern Analysis

The analysis of Land Surface Temperature (LST) across Kinshasa reveals a temperature range from 18°C to 27.83°C, with significant spatial variability. The highest temperatures were concentrated in the eastern and southern parts of the city, while lower temperatures were predominantly found in the western and northern regions. Several factors could potentially contribute to this variation in LST values, including vegetation cover, proximity to water bodies, industrialization, and urbanization. According to Bindajam et

al. (2020), areas with dense vegetation tend to exhibit lower LST values due to the cooling effects generated by plant transpiration and shading. They further explained that dense vegetation both blocks incoming solar radiation and cools the surface by evaporating water from leaves, leading to significantly cooler ground temperatures compared to sparse or built-up areas. This is evident in the western parts of Kinshasa, where the presence of the Congo River and surrounding vegetation plays a crucial role in moderating temperatures. The Congo River functions as an urban cooling corridor, reducing nearby LST by 1–1.5 °C, and creates a more favorable microclimate that encourages settlements which is evidenced by enhanced urbanization along its banks (Chen et al. 2014; Guo et al. 2023). However, despite the cooling effect of the river, the western regions near the Congo River also show high LST values due to the dense population and associated anthropogenic activities. Vujovic et al. (2021) confirmed that urban areas, particularly those with minimal vegetation and high population density, contribute to the UHI effect, where built-up surfaces absorb and retain heat, leading to increased LST values. Furthermore, the eastern and southern parts of Kinshasa, characterized by significant agricultural activities (Mufungizi et al. 2023), show higher LST values. The clearing of land for agriculture in these regions reduces vegetation cover, thereby increasing surface temperatures. This pattern highlights the impact of land use changes on the thermal environment of the city (Ebode 2023).

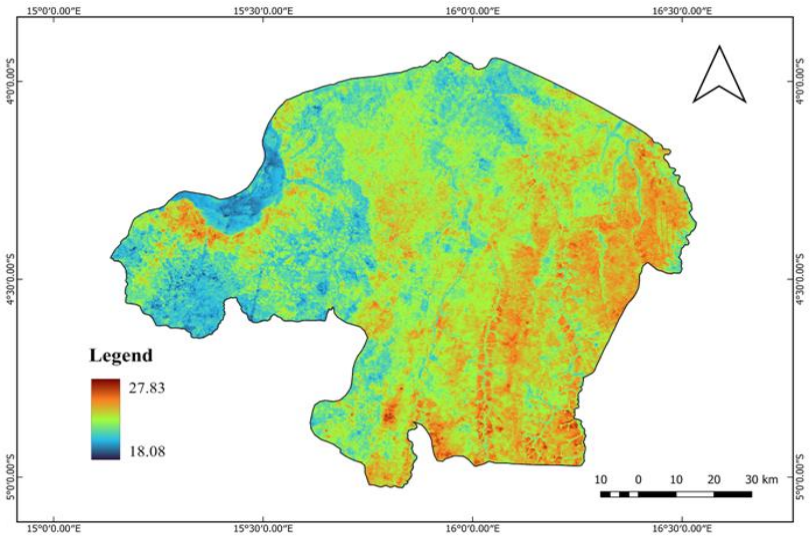


*Figure 3: Spatial distribution of median LST (2013-2023) in Kinshasa – prepared by Author using GEE & QGIS*

## NDVI Spatial Pattern Analysis

The Normalized Difference Vegetation Index (NDVI) for Kinshasa reveals a wide range of vegetative greenness, from 0.87 to 0.1 (Figure 4). This variation highlights significant differences in vegetation cover across the city. Mont-Ngafula and Maluku municipalities stand out with NDVI values of 0.69 and 0.64, respectively, indicating substantial vegetation cover in these areas. In contrast, Ngiri-Ngiri and Ngaba municipalities exhibit lower NDVI values of 0.32 and 0.34, respectively, primarily due to extensive built-up areas and urban development (Kabanyegeye et al. 2024). In the southwestern part of Kinshasa, notable vegetation is observed, particularly along the Nsele River. This region benefits from a higher tree cover, which is essential for cooling and mitigating urban heat effects. The presence of significant green spaces in this area contributes to a more moderate LST compared to more densely built-up regions (Bindajam et al.

2020). To the northeast of Kinshasa, the Mampu agroforestry plantations demonstrate another critical aspect of vegetation cover. These plantations, predominantly consisting of Acacia auriculiformis woodlands and areas dedicated to cassava production (Péroches et al. 2022), exhibit NDVI values ranging from 0.44 to 0.69.

The spatial distribution of NDVI values underscores the influence of both natural and anthropogenic factors on vegetation patterns in Kinshasa and how it may affect the distribution of heat risk (Mufungizi et al. 2023; IPCC 2022). Areas with high NDVI values, such as Mont-Ngafula and Maluku, contribute positively to local climate regulation by providing shade and reducing heat absorption and hence low vulnerability. Conversely, regions with lower NDVI values, such as Ngiri-Ngiri and Ngaba, reflect the impact of urbanization on vegetation cover, leading to increased heat retention and higher LST and high vulnerability to heat risk (Vujovic et al. 2021). Generally, the NDVI spatial patterns is an indication of the varying degrees of vegetation cover across Kinshasa and its implications for urban heat dynamics. Understanding these patterns is essential for developing strategies to enhance green spaces and improve urban resilience to heat risk.

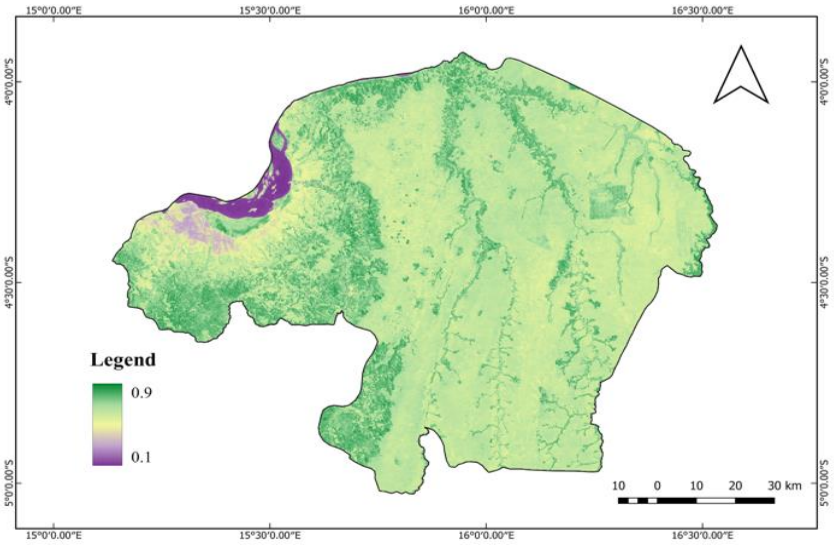


***Figure 4: Spatial distribution of median NDVI (2013-2023) in Kinshasa – prepared by Author using GEE & QGIS***

**Population Density (<10 & >65) Spatial Pattern Analysis**

In Kinshasa, areas with high populations of individuals in vulnerable age groups were mainly found in densely populated urban centers and settlements, particularly in the western part of the city as shown in Figure 5. Bumbu and Ngaba municipalities had the highest concentrations of people aged below 10 and above 65, whereas Maluku and Nsele municipalities had the lowest populations in this age range. The high population influx of people has largely been attributed to the increase in population growth in Kinshasa (Batana et al. 2021a) with Anglewicz (2017) suggesting that the in-migrants high fertility also contributed to Kinshasa's fast population.

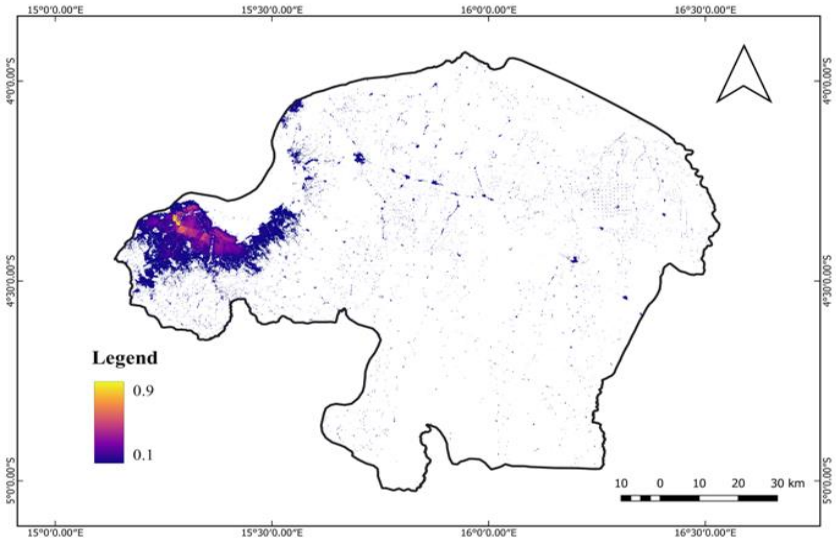


*Figure 5: Spatial distribution of vulnerable age groups (<10 & >65 years) in Kinshasa – prepared by Author using QGIS*

**Spatial Distribution of Risk Components**

The three risk components derived from the selected indicators were classified into five categories (very low, low, medium, high, and very high) using the "Natural Breaks" technique. Their spatial distributions were depicted in Figure 6, with the thresholds that defined the categories for each component displayed behind the categories accordingly.

*Hazard*

Figure 6(a) shows that low-hazard areas ("very low" and "low") are mainly located in the western part of Kinshasa, while high-hazard areas ("high" and "very high") are concentrated in the eastern and southeastern regions. The elevated heat hazard in the eastern areas corresponds to sparse vegetation cover, which reduces natural cooling through evapotranspiration (Bowler et al., 2010; Li et al., 2017). In the western region, high hazard zones are primarily in the dense urban core where built-up surfaces dominate, vegetation is minimal, and Land Surface Temperature (LST) is elevated. The city's periphery, characterized by higher vegetation density, shows low to medium heat hazard, highlighting the strong inverse relationship between vegetation cover and surface temperature (Voogt & Oke, 2003; IPCC, 2022). This pattern aligns with established Urban Heat Island (UHI) theory, which attributes higher urban temperatures to impervious surfaces and reduced greenery (Oke, 1982; Vujovic et al., 2021). These findings underscore the potential of urban greening strategies, such as tree planting, to mitigate heat hazard by lowering LST and improving urban microclimates (Li et al., 2017; Bowler et al., 2010).

**Exposure**

The spatial distribution of heat exposure in Kinshasa, presented in Figure 6(b), reveals a pronounced concentration of high-exposure zones within the densely populated urban core. Areas such as Kasa-Vubu, Ngiri-Ngiri, and Bumbu exhibit very high exposure levels, which can be attributed to both the high population density and the limited vegetation cover observed in these districts. This pattern aligns with the findings of Obe et al. (2023), who demonstrated that exposure to climate-related risks such as extreme heat

is strongly correlated with urban population density and land-use characteristics. Urban centers like Kinshasa experience elevated exposure due to intense in-migration from rural regions, as people seek better access to employment, commerce, education, and infrastructure. This internal migration trend, driven by socioeconomic push-pull factors, leads to the rapid expansion of informal settlements and high-density neighbourhoods with inadequate green infrastructure (Nsokimieno et al., 2010; UN-Habitat, 2020). These areas often lack tree cover and open spaces, exacerbating exposure to urban heat island effects and intensifying residents' vulnerability to extreme heat events (Kabisch et al., 2016; IPCC, 2022).

Moreover, the spatial clustering of high exposure zones within Kinshasa reflects typical urbanization trends seen in many sub-Saharan African cities, where rapid urban growth outpaces planning and infrastructure development (Dodman, 2009; Simon et al., 2016). As noted by Mufungizi & Akilimali (2024), Kinshasa's demographic expansion has been most intense in its urban core, where economic activity is concentrated and where land pressure limits the inclusion of climate-adaptive features such as parks and urban forests.

In contrast, the peripheral and rural parts of Kinshasa show predominantly low exposure levels. These areas are more sparsely populated and typically characterized by larger plots of land per household, greater vegetation coverage, and lower impervious surface ratios. As such, they are less affected by anthropogenic heat accumulation, which contributes to a lower population exposure to heat stress (López-Bueno et al., 2021; Van de Walle et al., 2022).

Overall, the exposure distribution across Kinshasa mirrors broader urban environmental justice challenges, whereby poorer, densely populated communities are often more exposed to climate hazards due to structural inequalities in land use, housing, and access to green infrastructure (Harlan et al., 2006; Rufat et al., 2015).

*Vulnerability*

The spatial distribution of vulnerability across Kinshasa reveals critical disparities linked to population demographics, infrastructure, and vegetation cover. High vulnerability is concentrated in the western parts of the city, particularly in densely populated neighbourhoods like Bumbu and northern Selembao. These areas house a significant proportion of age-dependent populations (children under 10 and adults over 65) (Figure 5), who are more physiologically susceptible to extreme heat, as identified in previous studies (Uejio et al., 2011; Harlan et al., 2006). Moreover, these regions exhibit sparse vegetation (Figure 4), exacerbating exposure to urban heat due to the lack of cooling from green infrastructure (Li et al., 2017; IPCC, 2022). Many residents in these areas live in informal settlements or low-income conditions and have limited access to adaptive measures such as electric fans or air conditioning. This aligns with findings by Batana et al. (2021b), who noted that poverty in Kinshasa is disproportionately concentrated in inner-city neighbourhoods, leaving populations more vulnerable to environmental stressors. Similarly, Rufat et al. (2015) emphasized that vulnerability to climate hazards is amplified by pre-existing socioeconomic inequalities, especially in poorly planned urban settings.

Conversely, neighbourhoods with better infrastructure and socioeconomic conditions—often on the city's periphery—demonstrate lower vulnerability. These areas benefit from more deliberate urban planning, greater access to cooling technologies, and relatively higher vegetation coverage, all of which reduce sensitivity to heat extremes (IPCC, 2022; Kabisch et al., 2016). In other parts of Kinshasa, including sections of the north, east, and south, vulnerability levels tend to be moderate and spatially fragmented.

These zones are partially buffered by adjacent vegetation and less intense urban development, which collectively mitigate the intensity of heat risk (López-Bueno et al., 2021).

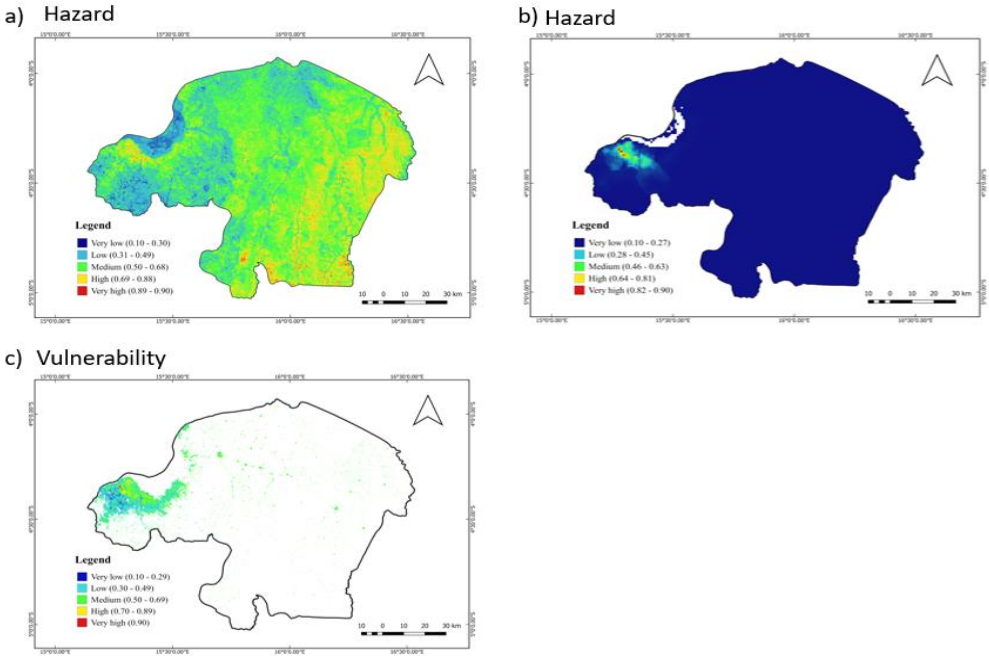


*Figure 6: (a) Spatial distribution of heat hazard, (b) heat exposure, and (c) heat vulnerability*

**Spatial Distribution of the Final Heat Risk Layer**

The integration of hazard, exposure, and vulnerability components using a multiplicative framework revealed clear spatial variations in heat-related risk across Kinshasa, DRC. The resulting heat risk map (Figure 7) displays a distinct spatial gradient, with lower risk levels concentrated along the city's periphery and higher risk levels prevailing in central urban zones. This pattern is consistent with the urban heat vulnerability literature and can be understood through a combination of biophysical and socioeconomic determinants.

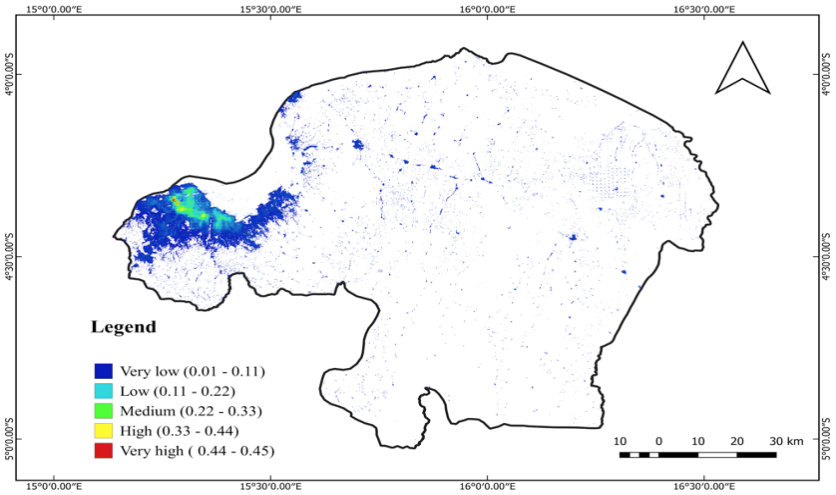


*Figure 7:. Final Heat risk map of Kinshasa DRC – prepared by Author using QGIS*

Peripheral areas of Kinshasa generally exhibit low to very-low heat risk. This reduced risk correlates with several protective factors identified in urban climate vulnerability studies. First, these areas tend to be wealthier and more spaciously planned, enabling access to adaptive measures such as air conditioning, electric fans, and well-ventilated buildings—critical tools for mitigating heat stress (Batana et al., 2021b; IPCC, 2022; Rufat et al., 2015). The relationship between affluence and lower heat vulnerability has been extensively documented. For instance, Harlan et al. (2006) found that higher-income neighbourhoods in Phoenix, Arizona, were systematically less exposed to extreme heat due to better infrastructure, vegetative cover, and access to cooling appliances. Similar results were reported in South Africa, where Pasquini et al. (2020) showed that suburban communities experienced less heat-related discomfort owing to higher socioeconomic capital and better housing design. Vegetation also plays a crucial role in modulating local temperatures and thereby influencing heat risk. The peripheral zones of Kinshasa are characterized by higher NDVI values, which signify dense vegetation cover. Numerous studies have linked vegetation to microclimate regulation via evapotranspiration and shading effects (Zhang et al., 2016; Van de Walle et al., 2022). These findings support the observed lower LST and risk levels in greener, less urbanized neighbourhoods.

In contrast, the central districts of Kinshasa exhibit medium to very-high heat risk levels. These areas are typified by high population densities, limited vegetation, and widespread informal settlements—factors that collectively increase both exposure and vulnerability. Slum communities often lack access to reliable electricity, ventilation, and cooling appliances, exacerbating susceptibility to heat stress (Hugo & Sonnendecker, 2023). Comparable results have been observed in other African cities, where informal urban zones are disproportionately affected by thermal extremes due to limited adaptive capacity (Tusting et al., 2019; Olazabal et al., 2021). Moreover, Uejio et al. (2011) emphasize that densely populated, low-income areas often concentrate heat risk due to higher ambient temperatures and poorer housing conditions. The rural hinterlands surrounding Kinshasa, in contrast, tend to display very-low risk levels. These regions benefit from lower exposure due to sparse population density and reduced urban heat island effects. Similar trends have been reported in other tropical settings; López-Bueno et al. (2021) found that rural residents in sub-Saharan Africa were generally less exposed to heat-related morbidity due to more dispersed settlements and the cooling influence of surrounding vegetation.

Overall, the spatial heat risk distribution in Kinshasa reveals a concentric pattern of decreasing risk with distance from the urban core. This gradient aligns with findings from previous studies in diverse geographies—ranging from Accra to Delhi—where heat risk is shaped by complex interactions among social inequality, environmental factors, and infrastructure (Ma et al., 2023; Dong et al., 2020; Hajat & Kosatky, 2010). The corroboration from this literature reinforces the robustness of the observed patterns in Kinshasa and underscores the urgent need for spatially targeted heat adaptation strategies in highly vulnerable urban neighbourhoods.

## Conclusion

This study investigates the spatial distribution of various environmental and human factors and how they interplay to give insight into the underlying heat risk in the study area. The spatial distribution of LST in Kinshasa reflects a complex interplay of natural and anthropogenic factors. Lower LST values in the western and northern regions are strongly associated with dense vegetation and proximity to the Congo River, which provide cooling effects through evapotranspiration and water regulation. Conversely, the

eastern and southern parts exhibit higher LST values, largely driven by agricultural land clearing and reduced vegetation cover. The spatial distribution of NDVI in Kinshasa reveals clear disparities in vegetation cover influenced by both natural landscapes and human activities. These variations directly impact local LST and vulnerability to heat, emphasizing the critical role of urban greening in enhancing climate resilience and mitigating heat-related risks across the city.

The study also highlights a clear demographic concentration of vulnerable age groups in the densely populated western urban centers of Kinshasa, particularly in Bumbu and Ngaba while peripheral municipalities such as Maluku and Nsele exhibit lower population densities and fewer individuals in sensitive age categories. Ultimately, the spatial distribution of heat risk in Kinshasa reveals a clear urban-to-rural gradient, with very-high to medium risk levels concentrated in the densely populated and socioeconomically disadvantaged central urban areas, and low to very-low risk levels found in the peripheral and rural regions. This pattern highlights the critical role of socioeconomic status, vegetation cover, infrastructure quality, and population density in shaping heat risk.

As a pioneering study in Central Africa, this research faced several limitations. Data constraints restricted the analysis to a limited set of indicators, including NDVI, RWI, LST, and population density. Future assessments of heat-related health risks should incorporate additional socioeconomic factors, such as the proportion of people with disabilities (Paranunzio et al., 2021), the number of air conditioners per household (Hu et al., 2017; Chen et al., 2018), and the availability of hospital beds (Chen et al.2018; Zhang et al., 2019). These factors could provide a more comprehensive understanding of exposure and vulnerability. Additionally, the RWI data, acquired with a resolution of approximately 2400 meters and presented as point features, were rasterized using the Kriging method, which assumes spatial autocorrelation. This assumption may introduce uncertainties, particularly due to the limited number of data points and the coarse resolution.

Despite these limitations, the study found that central urban areas of Kinshasa are at higher risk for heat-related health issues compared to the urban periphery and rural areas. The high vulnerability of urban populations, characterized by dense living conditions and lower socioeconomic status, significantly contributes to this heightened risk. While some research suggests that rural areas might face greater heat risks (Hu et al., 2017), our findings align with studies indicating that high dense urban areas can be extremely vulnerable to heat, given factors like urban poverty, congestion, and inadequate health infrastructure (Aubrecht et al., 2013). The research also highlighted that densely populated areas pose the greatest health risk from heat exposure. In order to address this, there is a need for mitigation strategies to focus on reducing exposure levels, particularly in Kinshasa's densely populated districts. The government should Implement urban forestry programs by planting trees along streets and markets especially in high-risk urban zones like Ngaba, subsidize low-energy cooling technologies for low-income households and make heat risk mapping and modeling a standard input into land use planning, housing policy, and infrastructure development. This aligns with broader adaptation and mitigation plans aimed at minimizing health risks related to extreme heat (IPCC, 2012; IPCC, 2014). This study provides important insights into the spatial distribution of health-related heat risk in Kinshasa which offers valuable information for policymakers to develop targeted adaptation and mitigation strategies tailored to the reality of the most vulnerable areas.

## References

Abrar, R., Sarkar, S. K., Nishtha, K. T., Talukdar, S., Shahfahad, Rahman, A., & Mosavi, A. (2022). Assessing the spatial mapping of heat vulnerability under urban heat island (UHI) effect in the Dhaka Metropolitan Area. *Sustainability, 14*(9), 4945. https://doi.org/10.3390/su14094945

Adegun, O. B., & Ayoola, H. A. (2021). Between the rich and poor: Exposure and adaptation to heat stress across two urban neighbourhoods in Nigeria. *Environment, Development and Sustainability, 24*(10), 11953–11968. https://doi.org/10.1007/s10668-021-01924-w

AFRISTAT & National Institute of Statistics (Congo, DR). (2012). *Democratic Republic of the Congo 1-2-3 Survey on Employment, the Informal Sector, and Household Living Conditions 2012*.

Anglewicz, P., Corker, J., & Kayembe, P. (2017). The fertility of internal migrants to Kinshasa. *Genus, 73*(1), 4. https://doi.org/10.1186/s41118-017-0020-8

Aubrecht, C., & Özceylan, D. (2013). Identification of heat risk patterns in the US national capital region by integrating heat stress and related vulnerability. *Environment International, 56*, 65–77. https://doi.org/10.1016/j.envint.2013.03.005

Avdan, U., & Jovanovska, G. (2016). Algorithm for automated mapping of land surface temperature using LANDSAT 8 satellite data. *Journal of Sensors, 2016*, 1480307. https://doi.org/10.1155/2016/1480307

Ayal, D. Y. (2021). Climate change and human heat stress exposure in sub-Saharan Africa. *CABI Reviews, 2021*(049). https://doi.org/10.1079/pavsnnr202116049

Bao, J., Li, X., & Yu, C. (2015). The construction and validation of the heat vulnerability index: A review. *International Journal of Environmental Research and Public Health, 12*(7), 7220–7234. https://doi.org/10.3390/ijerph120707220

Batana, Y. M., Jarotschkin, A., Konou, A., Masaki, T., Nakamura, S., & Viboudoulou Vilpoux, M. E. (2021a). *Profiling living conditions of the DRC urban population: Access to housing and services in Kinshasa Province* (Policy Research Working Paper No. 9857). The World Bank. https://doi.org/10.1596/1813-9450-9857

Batana, Y. M., Masaki, T., Nakamura, S., & Viboudoulou Vilpoux, M. E. (2021b). *Estimating poverty in Kinshasa by dealing with sampling and comparability issues* (Policy Research Working Paper No. 9858). The World Bank. https://doi.org/10.1596/1813-9450-9858

Bindajam, A. A., Mallick, J., AlQadhi, S., Singh, C. K., & Hang, H. T. (2020). Impacts of vegetation and topography on land surface temperature variability over the semi-arid mountain cities of Saudi Arabia. *Atmosphere, 11*(7), 762. https://doi.org/10.3390/atmos11070762

Bolin, B., Nelson, A., Hackett, E. J., Pijawka, K. D., Sicotte, D., Sadalla, E. K., Matranga, E., & O'Donnell, M. (2002). The ecology of technological risk in a Sunbelt city. *Environment and Planning A: Economy and Space, 34*(2), 317–339. https://doi.org/10.1068/a34125

Bowler, D. E., Buyung-Ali, L., Knight, T. M., & Pullin, A. S. (2010). Urban greening to cool towns and cities: A systematic review of the empirical evidence. *Landscape and Urban Planning, 97*(3), 147–155. https://doi.org/10.1016/j.landurbplan.2010.05.006

Buscail, C., Upegui, E., & Viel, J. F. (2012). Mapping heatwave health risk at the community level for public health action. *International Journal of Health Geographics, 11*(1), 38. https://doi.org/10.1186/1476-072X-11-38

Campbell, S., Remenyi, T. A., White, C. J., & Johnston, F. H. (2018). Heatwave and health impact research: A global review. *Health & Place, 53*, 210–218. https://doi.org/10.1016/j.healthplace.2018.08.017

Chen, B., Xie, M., Feng, Q., Wu, R., & Jiang, L. (2022). Diurnal heat exposure risk mapping and related governance zoning: A case study of Beijing, China. *Sustainable Cities and Society, 81*, 103831. https://doi.org/10.1016/j.scs.2022.103831

Chen, Q., Ding, M. J., Yang, X. C., Hu, K. J., & Qi, J. G. (2018). Spatially explicit assessment of heat health risk by using multi-sensor remote sensing images and socioeconomic data in Yangtze River Delta, China. *International Journal of Health Geographics, 17*(1), 1–15. https://doi.org/10.1186/s12942-018-0145-9

Chen, Y. C., Tan, C. H., Wei, C., & Su, Z. W. (2014). Cooling effect of rivers on metropolitan Taipei using remote sensing. *International Journal of Environmental Research and Public Health, 11*(2), 1195–1210. https://doi.org/10.3390/ijerph110201195

Chirisa, I., Matamanda, A., & Mukarwi, L. (2017). Desired and achieved urbanisation in Africa: In search of appropriate tooling for a sustainable transformation. In U. Benna & I. Benna (Eds.), *Urbanization and its impact on socio-economic growth in developing regions* (pp. 101–102). IGI Global.

Collins, T., Grineski, S., & Aguilar, M. (2009). Vulnerability to environmental hazards in the Ciudad Juárez (Mexico)–El Paso (USA) metropolis: A model for spatial risk assessment in transnational context. *Applied Geography, 29*(3), 448–461. https://doi.org/10.1016/j.apgeog.2009.03.005

Costello, J. T., Rendell, R. A., Furber, M., Massey, H. C., Tipton, M. J., Young, J. S., & Jay, O. (2018). Effects of acute or chronic heat exposure, exercise and dehydration on plasma cortisol, IL-6 and CRP levels in trained males. *Cytokine, 110*, 277–283. https://doi.org/10.1016/j.cyto.2018.01.018

Crichton, D. (1999). The risk triangle. In J. Ingleton (Ed.), *Natural disaster management* (pp. 102–103). Tudor Rose.

Defries, R. S., & Townshend, J. R. G. (1994). NDVI-derived land cover classifications at a global scale. *International Journal of Remote Sensing, 15*(17), 3567–3586. https://doi.org/10.1080/01431169408954345

Deryng, D., Conway, D., Ramankutty, N., Price, J., & Warren, R. (2014). Global crop yield response to extreme heat stress under multiple climate change futures. *Environmental Research Letters, 9*(3), 034011. https://doi.org/10.1088/1748-9326/9/3/034011

Diffenbaugh, N. S., & Burke, M. (2019). Global warming has increased global economic inequality. *Proceedings of the National Academy of Sciences, 116*(20), 9808–9813. https://doi.org/10.1073/pnas.1816020116

Dodman, D. (2009). Blaming cities for climate change? An analysis of urban greenhouse gas emissions inventories. *Environment and Urbanization, 21*(1), 185–201. https://doi.org/10.1177/0956247809103016

Dong, J., Peng, J., He, X., Corcoran, J., Qiu, S., & Wang, X. (2020). Heatwave-induced human health risk assessment in megacities based on heat stress-social vulnerability-human exposure framework. *Landscape and Urban Planning, 203*, 103907. https://doi.org/10.1016/j.landurbplan.2020.103907

Dong, W. H., Liu, Z., Zhang, L., Tang, Q. H., Liao, H., & Li, X. E. (2014). Assessing heat health risk for sustainability in Beijing's urban heat island. *Sustainability, 6*(10), 7334–7357. https://doi.org/10.3390/su6107334

Dosio, A. (2017). Projection of temperature and heat waves for Africa with an ensemble of CORDEX regional climate models. *Climate Dynamics, 49*(1–2), 493–519. https://doi.org/10.1007/s00382-016-3355-5

Ebode, V. B. (2023). Land surface temperature variation in response to land use modes changes: The case of Mefou River Sub-Basin (Southern Cameroon). *Sustainability, 15*(1), 864. https://doi.org/10.3390/su15010864

Epule, T. E., Chehbouni, A., Dhiba, D., & Moto, M. W. (2021). The readiness index for climate change adaptation in Africa: The role of climate and adaptive capacity proxies. *Applied Sciences, 11*(20), 9413. https://doi.org/10.3390/app11209413

Fedeski, M., & Gwilliam, J. (2007). Urban sustainability in the presence of flood and geological hazards: The development of a GIS-based vulnerability and risk assessment methodology. *Landscape and Urban Planning, 83*(1), 50–61. https://doi.org/10.1016/j.landurbplan.2007.05.004

Flouriot, J. (2013). Kinshasa 2005. Trente ans après la publication de l'Atlas de Kinshasa. *Les Cahiers d'Outre-Mer, 66*(261), 5–28. https://doi.org/10.4000/com.6770

Forzieri, G., Feyen, L., Russo, S., Vousdoukas, M., Alfieri, L., Outten, S., Migliavacca, M., Bianchi, A., Rojas, R., & Cid, A. (2018). Escalating impacts of climate extremes on critical infrastructures in Europe. *Global Environmental Change, 48*, 97–107. https://doi.org/10.1016/j.gloenvcha.2017.11.007

Guo, F., Xu, S., Zhao, J., Zhang, H., Liu, L., Zhang, Z., & Yin, X. (2023). Study on the mechanism of urban morphology on river cooling effect in severe cold regions. *Frontiers in Public Health, 11*, 1170627. https://doi.org/10.3389/fpubh.2023.1170627

Harlan, S. L., Brazel, A. J., Prashad, L., Stefanov, W. L., & Larsen, L. (2006). Neighborhood microclimates and vulnerability to heat stress. *Social Science & Medicine, 63*(11), 2847–2863. https://doi.org/10.1016/j.socscimed.2006.07.030

Harris, R. M. B., Beaumont, L. J., Vance, T. R., Tozer, C. R., Remenyi, T. A., Perkins-Kirkpatrick, S. E., Mitchell, P. J., Nicotra, A. B., McGregor, S., Andrew, N. R., Letnic, M., Kearney, M. R., Wernberg, T., Hutley, L. B., Chambers, L. E., Fletcher, M.-S., Keatley, M. R., Woodward, C. A., Williamson, G., … Bowman, D. M. J. S. (2018). Biological responses to the press and pulse of climate trends and extreme events. *Nature Climate Change, 8*(7), 579–587. https://doi.org/10.1038/s41558-018-0187-9

Hajat, S., & Kosatky, T. (2010). Heat-related mortality: A review and exploration of heterogeneity. *Journal of Epidemiology & Community Health, 64*(9), 753–760. https://doi.org/10.1136/jech.2009.087999

Heaviside, C., Macintyre, H., & Vardoulakis, S. (2017). The urban heat island: Implications for health in a changing environment. *Current Environmental Health Reports, 4*(3), 296–305. https://doi.org/10.1007/s40572-017-0150-3

He, C., Ma, L., Zhou, L., Kan, H., Zhang, Y., Ma, W., & Chen, B. (2019). Exploring the mechanisms of heat wave vulnerability at the urban scale based on the application of big data and artificial societies. *Environment International, 127*, 573–583. https://doi.org/10.1016/j.envint.2019.01.057

Hugo, J. M., & Sonnendecker, P. W. (2023). Ground-level documentation of heat stress exposure and response strategies in informal settlements in Tshwane, South Africa. *Smart and Sustainable Built Environment.* Advance online publication. https://doi.org/10.1108/SASBE-03-2023-0059

Hu, L., Wilhelmi, O. V., & Uejio, C. (2019). Assessment of heat exposure in cities: Combining the dynamics of temperature and population. *Science of The Total Environment, 655*, 1–12. https://doi.org/10.1016/j.scitotenv.2018.11.028

IPCC. (2012). *Managing the risks of extreme events and disasters to advance climate change adaptation* [Special report]. Cambridge University Press. https://doi.org/10.1017/CBO9781139177245

IPCC. (2014). *Climate change 2014: Impacts, adaptation, and vulnerability* [Contribution of Working Group II to the Fifth Assessment Report]. Cambridge University Press.

IPCC. (2021). *Climate change 2021: The physical science basis* [Contribution of Working Group I to the Sixth Assessment Report]. Cambridge University Press.

IPCC. (2022). *Climate change 2022: Impacts, adaptation, and vulnerability* [Contribution of Working Group II to the Sixth Assessment Report] (pp. 3–33). Cambridge University Press.

Kabanyegeye, H., Cirezi, N. C., Muteya, H. K., Mbarushimana, D., Mukubu Pika, L., Salomon, W., Useni Sikuzani, Y., Sambieni, K. R., Masharabu, T., & Bogaert, J. (2024). Spatio-temporal analysis of green infrastructure along the urban-rural gradient of the cities of Bujumbura, Kinshasa and Lubumbashi. *Land, 13*(9), 1467. https://doi.org/10.3390/land13091467

Kabisch, N., Qureshi, S., & Haase, D. (2016). Human–environment interactions in urban green spaces—A systematic review of contemporary issues and prospects for future research. *Environmental Impact Assessment Review, 50*, 25–34. https://doi.org/10.1016/j.eiar.2014.08.007

Kang, L., Li, Y., Hu, S., Chen, M., Yang, C., Yang, B. X., Wang, Y., Hu, J., Lai, J., Ma, X., Chen, J., Guan, L., Wang, G., Ma, H., & Liu, Z. (2020). The mental health of medical workers in Wuhan, China dealing with the 2019 novel coronavirus. *The Lancet Psychiatry, 7*(4), e14. https://doi.org/10.1016/S2215-0366(20)30047-X

Kenny, G. P., Wilson, T. E., Flouris, A. D., & Fujii, N. (2018). Heat exhaustion. In *Handbook of clinical neurology* (1st ed., Vol. 157, pp. 505–529). Elsevier. https://doi.org/10.1016/B978-0-444-64074-1.00031-8

Kerstin, F., Stefan, S., Philip, B., Buth, M., & Kahlenborn, M. (2017). *The Vulnerability Sourcebook: Concept and guidelines for standardized vulnerability assessments*. Deutsche Gesellschaft für Internationale Zusammenarbeit (GIZ). https://www.adaptationcommunity.net/download/va/vulnerability-guidesmanualsreports/vuln_source_2017_EN.pdf

Kinyamb, S., Nsenda, F., Nonga, D., Kaminar, T., & Mbalanda, W. (2015). *Monographie de la ville de Kinshasa, Democratic Republic of Congo*. Institut Congolais de Recherche en Développement et Etudes Stratégiques (ICREDES).

Lapola, D. M., Braga, D. R., Di Giulio, G. M., Torres, R. R., & Vasconcellos, M. P. (2019). Heat stress vulnerability and risk assessment at the (super) local scale in six Brazilian capitals. *Climatic Change, 154*(3–4), 477–492. https://doi.org/10.1007/s10584-019-02459-w

Li, X., Zhou, Y., Asrar, G. R., Mao, J., Li, X., & Li, W. (2017). Response of vegetation phenology to urbanization in the conterminous United States. *Global Change Biology, 23*(7), 2818–2830. https://doi.org/10.1111/gcb.13562

López-Bueno, J. A., Navas-Martín, M. A., Díaz, J., Mirón, I. J., Luna, M. Y., Sánchez-Martínez, G., Culqui, D., & Linares, C. (2021). Analysis of vulnerability to heat in rural and urban areas in Spain: What factors explain heat's geographic behavior? *Environmental Research, 207*, 112213. https://doi.org/10.1016/j.envres.2021.112213

Loughnan, M. E., Tapper, N. J., Phan, T., & McInnes, J. A. (2014). Can a spatial index of heat-related vulnerability predict emergency service demand in Australian capital cities? *International Journal of Emergency Services, 3*(1), 6–33. https://doi.org/10.1108/IJES-03-2013-0007

Luber, G., & McGeehin, M. (2008). Climate change and extreme heat events. *American Journal of Preventive Medicine, 35*(5), 429–435. https://doi.org/10.1016/j.amepre.2008.08.021

Ma, L., Huang, G., Johnson, B. A., Chen, Z., Li, M., Yan, Z., Zhan, W., Lu, H., He, W., & Lian, D. (2023). Investigating urban heat-related health risks based on local climate zones: A case study of Changzhou in China. *Sustainable Cities and Society, 91*, 104402. https://doi.org/10.1016/j.scs.2023.104402

Maragno, D., Dalla Fontana, M., & Musco, F. (2020). Mapping heat stress vulnerability and risk assessment at the neighborhood scale to drive urban adaptation planning. *Sustainability, 12*(3), 1056. https://doi.org/10.3390/su12031056

Morabito, M., Crisci, A., Gioli, B., Gualtieri, G., Toscano, P., Di Stefano, V., & Orlandini, S. (2015). Urban-hazard risk analysis: Mapping of heat-related risks in the elderly in major Italian cities. *PLOS ONE, 10*(5), e0127277. https://doi.org/10.1371/journal.pone.0127277

Morakinyo, T. E., Ishola, K. A., Eresanya, E. O., Daramola, M. T., & Balogun, I. A. (2024). Spatio-temporal characteristics of heat stress over Nigeria using evaluated ERA5-HEAT reanalysis data. *Weather and Climate Extremes, 45*, 100704. https://doi.org/10.1016/j.wace.2024.100704

Morrison, C., & Shortt, N. (2008). Fuel poverty in Scotland: Refining spatial resolution in the Scottish Fuel Poverty Indicator using a GIS-based multiple risk index. *Health & Place, 14*(4), 702–717. https://doi.org/10.1016/j.healthplace.2007.11.003

Mufungizi, I., Kawaya, T., Bongeli, R., Kabulo, J., Diakondua, R., & Ruben, L. L. (2023). Mapping and spatiotemporal dynamics of land-use and land-cover change based on the USGS and NASA platforms from MCD12Q1 Landsat imagery: A case study of Kinshasa, DR Congo. *International Journal of Advances in Scientific Research and Engineering, 9*(11), 61–72. https://doi.org/10.31695/IJASRE.2023.9.11.6

Mufungizi, I., & Akilimali, A. (2024). Control and orientation of urbanization of cities in developing countries: A case study of Kinshasa, Democratic Republic of the Congo. *Urban Planning and Transport Research, 12*(1), 2307350. https://doi.org/10.1080/21650020.2024.2307350

Nsokimieno, M., Shouyu, C., & Li, Z. (2010). Sustainable urbanization's challenge in Democratic Republic of Congo. *Journal of Sustainable Development, 3*(2), 242–254. https://doi.org/10.5539/jsd.v3n2p242

Obe, B., Morakinyo, T., & Mills, G. (2023). Assessing heat risk in a Sub-Saharan African humid city, Lagos, Nigeria, using numerical modelling and open-source geospatial socio-demographic datasets. *City and Environment Interactions, 20*, 100128. https://doi.org/10.1016/j.cacint.2023.100128

Obe, O. B., Morakinyo, T. E., & Mills, G. (2023). A study of the impact of landscape heterogeneity on surface energy fluxes in a tropical climate using SUEWS. *Urban Climate, 2*(1), 6–11. https://doi.org/10.1016/j.uclim.2023.101788

Odame, E. A., Li, Y., Zheng, S., Vaidyanathan, A., & Silver, K. (2018). Assessing heat-related mortality risks among rural populations: A systematic review and meta-analysis of epidemiological evidence. *International Journal of Environmental Research and Public Health, 15*(8), 1597. https://doi.org/10.3390/ijerph15081597

Oke, T. R. (1982). The energetic basis of the urban heat island. *Quarterly Journal of the Royal Meteorological Society, 108*(455), 1–24. https://doi.org/10.1002/qj.49710845502

Oudin Åström, D., Bertil, F., & Joacim, R. (2011). Heat wave impact on morbidity and mortality in the elderly population: A review of recent studies. *Maturitas, 69*(2), 99–105. https://doi.org/10.1016/j.maturitas.2011.03.008

Paranunzio, R., Dwyer, E., Fitton, J. M., Alexander, P. J., & O'Dwyer, B. (2021). Assessing current and future heat risk in Dublin city, Ireland. *Urban Climate, 40*, 100983. https://doi.org/10.1016/j.uclim.2021.100983

Pasquini, L., Aardenne, L. V., Godsmark, C. N., Lee, J., & Jack, C. (2020). Emerging climate change-related public health challenges in Africa: A case study of the heat-health vulnerability of informal settlement residents in Dar es Salaam, Tanzania. *Science of The Total Environment, 747*, 141355. https://doi.org/10.1016/j.scitotenv.2020.141355

Patz, J. A., Campbell-Lendrum, D., Holloway, T., & Foley, J. A. (2005). Impact of regional climate change on human health. *Nature, 438*(7066), 310–317. https://doi.org/10.1038/nature04188

Perkins, S. E., Alexander, L. V., & Nairn, J. R. (2012). Increasing frequency, intensity and duration of observed global heatwaves and warm spells. *Geophysical Research Letters, 39*(20), L20714. https://doi.org/10.1029/2012GL053361

Péroches, A., Baral, H., Chesnes, M., Lopez-Sampson, A., & Lescuyer, G. (2022). Suitability of large-scale tree plantation models in Africa, Asia and Latin America for forest landscape restoration objectives. *Bois et Forêts des Tropiques, 351*, 29–44. https://doi.org/10.19182/bft2022.351.a36870

Rana, I. A., Arshad, H. S. H., Jamshed, A., Khalid, Z., Younas, Z. I., Bhatti, S., & Ahmad, J. (2023). The impact of psychological distance to climate change and urban informality on adaptation planning. *Urban Climate, 49*, 101460. https://doi.org/10.1016/j.uclim.2023.101460

Rufat, S., Tate, E., Burton, C. G., & Maroof, A. S. (2015). Social vulnerability to floods: Review of case studies and implications for measurement. *International Journal of Disaster Risk Reduction, 14*(4), 470–486. https://doi.org/10.1016/j.ijdrr.2015.09.013

Su, J., Morello-Frosch, R., Jesdale, B. M., Kyle, A. D., Shamasunder, B., & Jerrett, M. (2009). An index for assessing demographic inequalities in cumulative environmental hazards with application to Los Angeles, California. *Environmental Science & Technology, 43*(20), 7626–7634. https://doi.org/10.1021/es901041p

Tan, J., Zheng, Y., Tang, X., Guo, C., Li, L., Song, G., Zhen, X., Yuan, D., Kalkstein, A. J., Li, F., & Chen, H. (2010). The urban heat island and its impact on heat waves and human health in Shanghai. *International Journal of Biometeorology, 54*(1), 75–84. https://doi.org/10.1007/s00484-009-0256-x

Taramelli, A., Melelli, L., Pasqui, M., & Sorichetta, A. (2008). Estimating hurricane hazards using a GIS system. *Natural Hazards and Earth System Sciences, 8*(4), 839–854. https://doi.org/10.5194/nhess-8-839-2008

Tomlinson, C. J., Chapman, L., Thornes, J. E., & Baker, C. J. (2011). Including the urban heat island in spatial heat health risk assessment strategies: A case study for Birmingham, UK. *International Journal of Health Geographics, 10*(1), 42. https://doi.org/10.1186/1476-072X-10-42

Uejio, C. K., Wilhelmi, O. V., Golden, J. S., Mills, D. M., Gulino, S. P., & Samenow, J. P. (2011). Intra-urban societal vulnerability to extreme heat: The role of heat exposure and the built environment,

socioeconomics, and neighborhood stability. *Health & Place, 17*(2), 498–507. https://doi.org/10.1016/j.healthplace.2010.12.005

UN-Habitat. (2020). *World cities report 2020: The value of sustainable urbanization*. United Nations Human Settlements Programme.

Van De Walle, J., Brousse, O., Arnalsteen, L., Brimicombe, C., Byarugaba, D., Demuzere, M., Kervyn, M., Lauwaet, D., Leyland, J., & Thiery, W. (2022). Lack of vegetation exacerbates exposure to dangerous heat in dense settlements in a tropical African city. *Environmental Research Letters, 17*(2), 024020. https://doi.org/10.1088/1748-9326/ac47c3

Voogt, J. A., & Oke, T. R. (2003). Thermal remote sensing of urban climates. *Remote Sensing of Environment, 86*(3), 370–384. https://doi.org/10.1016/S0034-4257(03)00079-8

Vujovic, S., Haddad, B., Karaky, H., Sebaibi, N., & Boutouil, M. (2021). Urban heat island: Causes, consequences, and mitigation measures with emphasis on reflective and permeable pavements. *CivilEng, 2*(2), 459–484. https://doi.org/10.3390/civileng2020026

Weng, Q., Lu, D., & Schubring, J. (2004). Estimation of land surface temperature–vegetation abundance relationship for urban heat island studies. *Remote Sensing of Environment, 89*(4), 467–483. https://doi.org/10.1016/j.rse.2003.11.005

Xu, H. Q. (2006). Modification of normalised difference water index (NDWI) to enhance open water features in remotely sensed imagery. *International Journal of Remote Sensing, 27*(14), 3025–3033. https://doi.org/10.1080/01431160600589179

Zhang, W., Zheng, C. G., & Chen, F. (2019). Mapping heat-related health risks of elderly citizens in mountainous areas: A case study of Chongqing, China. *Science of The Total Environment, 663*, 852–866. https://doi.org/10.1016/j.scitotenv.2019.01.395

Zhang, W., Zhu, Y., & Jiang, J. (2016). Effect of the urbanization of wetlands on microclimate: A case study of Xixi Wetland, Hangzhou, China. *Sustainability, 8*(9), 885. https://doi.org/10.3390/su8090885

Zheng, M., Zhang, J., Shi, L., Zhang, D., Sharma, T., & Prodhan, F. (2020). Mapping heat-related risks in northern Jiangxi Province of China based on two spatial assessment frameworks approaches. *International Journal of Environmental Research and Public Health, 17*(18), 6584. https://doi.org/10.3390/ijerph17186584